ARTICLE

Mechanistic Study of Initial Quenching Process in Photocatalytic α-Keto Acids Radical Acylation: A General Strategy for Enhancing Quantum Efficiency†

Zhicong Lin[a‡], Jialu Li[b‡], Chenli Chen[a], Linan Zhou[b*], Jialong Jie[a*], Hongmei Su[a*]

a. College of Chemistry, Beijing Normal University, Beijing 100890, China
b. School of Chemistry and Chemical Engineering, Spin-X Institute, South China University of Technology, Guangzhou 511442, China

(Dated: Received on July 31, 2024; Accepted on August 17, 2024)

The photocatalytic decarboxylation of α-keto acids to generate acyl radicals under mild conditions represents a novel strategy in organic synthesis. However, the quantum efficiency of this process has been underexplored, limiting its practicality. To improve quantum efficiency, detailed analysis of mechanisms and kinetic data for key steps are essential. In this work, using time-resolved emission and absorption spectroscopy, we conducted a mechanistic study focusing on the excited-state properties of representative photocatalysts and their quenching efficiencies during the initial quenching process ($[Ir(dFCF_3ppy)_2(dtbbpy)]^+$ (IrIII), Eosin Y (EY), Rose Bengal (RB), and 4CzPN). Our findings revealed that RB is active in its triplet states (^{3}RBH*), with lifetimes of 103 ns (in air) and 3.4 μs (in anaerobic conditions), while EY and 4CzPN are active in their singlet states (^{1}EYH* and ^{1}4CzPN*), with lifetimes of 2.9 ns and 5.1 ns, respectively. We measured the second-order rate constants for quenching by electron transfer from α-keto acids: ^{1}EYH*, 2.3×10^9 $(mol/L)^{-1}\cdot s^{-1}$; ^{3}RBH*, 3.2×10^8 $(mol/L)^{-1}\cdot s^{-1}$; ^{1}4CzPN*, 2.8×10^8 $(mol/L)^{-1}\cdot s^{-1}$. With our previously reported data for IrIII, we established the quenching efficiency relationships for these photocatalysts with α-keto acids concentration. Our steady-state chromatography experiments determined the quantum efficiencies for consumption of α-keto acids (IrIII > RBH > EYH > 4CzPN), correlating these efficiencies with the initial quenching process. The results suggest that IrIII/RBH under anaerobic conditions could be optimal for high quantum efficiency. This study provides a foundation for designing new photocatalytic α-keto acid radical acylation systems with enhanced quantum efficiency.

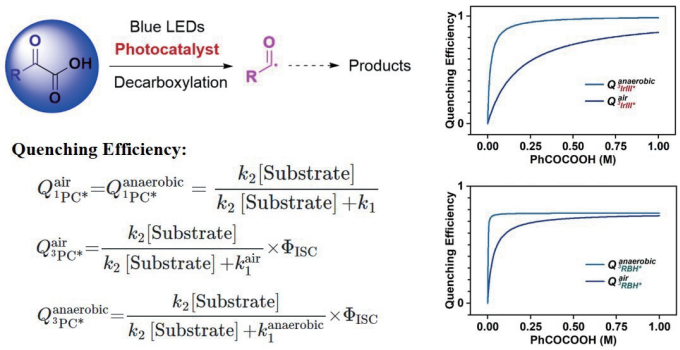

Key words: Chemical kinetics and dynamics, Time-resolved spectroscopy, Electron transfer quenching, Photocatalytic reaction

I. INTRODUCTION

Acyl radicals are highly reactive species that play a crucial role in organic synthesis chemistry, participating in a wide range of reactions [1]. Therefore, efficiently preparing acyl radical intermediates is essential for

† Part of Special Issue "In Memory of Prof. Xingxiao Ma on the occasion of his 90th Anniversary".
‡ These authors contributed equally to this work.
* Authors to whom correspondence should be addressed. E-mail: zhoulinan@scut.edu.cn, jialong@bnu.edu.cn, hongmei@bnu.edu.cn

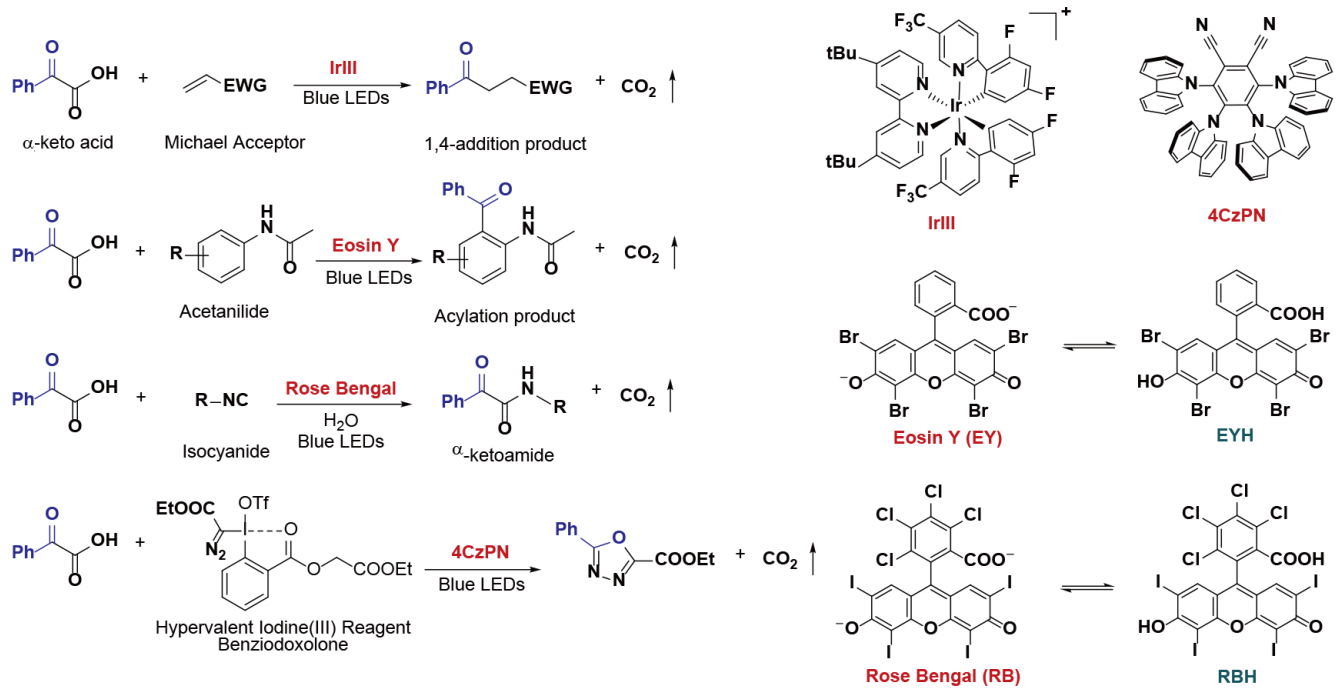

Scheme 1. Novel photocatalytic α-keto acids radical acylation reactions and the structures of photocatalysts used in these reactions.

synthesizing functional organic molecules. Compared to other acylating agents such as acyl chlorides and carbon monoxide, α-keto acids (RCOCOOH) offer advantages like structural stability and low toxicity, making them ideal acylating agents [1, 2]. In this context, the decarboxylation of RCOCOOH to generate acyl radicals has garnered significant attention [2]. However, most current methods require excess strong oxidants and/or high reaction temperatures. Consequently, developing a mild and environmentally friendly method to facilitate the decarboxylation of RCOCOOH holds significant research value. In recent years, photocatalytic reactions have become a green and practical synthetic technology [3]. Similarly, the photoredox catalytic RCOCOOH decarboxylation, which facilitates the easy formation of various carbonyl products under mild conditions, has recently been recognized as an appealing and promising method [4–16].

For example, in 2015, Fu *et al.* reported that iridium (Ir) photoredox catalysts facilitated the decarboxylative addition of RCOCOOH to olefine Michael acceptors [7]. This work introduced a novel acyl Michael addition, utilizing RCOCOOH to produce acyl anion via photocatalytic decarboxylation (Scheme 1). In the same year, Wang *et al.* presented a photocatalytic decarboxylative *ortho*-acylation of acetanilides with RCOCOOH using a dual catalytic system involving Eosin Y and Pd, which demonstrated a wide substrate scope and excellent functional group tolerance [8] (Scheme 1). In 2019, using Rose Bengal as the photocatalyst, Wei *et al.* unveiled a method for synthesizing α-ketoamides from RCOCOOH, involving photocatalytic promoting decarboxylation, radical addition, and hydration [13] (Scheme 1). In 2020, utilizing 4CzPN as the photocatalyst, Liu *et al.* described a photoredox catalytic route for preparing 2,5-disubstituted 1,3,4-oxadiazoles species via a decarboxylative cyclization reaction of RCOCOOH, which involved the coupling of radical intermediates to construct new C–N/C–O bonds [17] (Scheme 1).

From the perspective of synthetic methodology, photocatalytic systems need to consider the sustainability of the reaction, with high quantum efficiency being essential [18, 19]. However, despite the rapid expansion of reaction systems for implementing various photocatalytic α-keto acid decarboxylation-mediated radical acylation systems, quantum efficiencies have typically been overlooked and not optimized. In principle, such photocatalytic reactions often involve multiple highly reactive transient species, including excited states and radicals, and various reaction pathways [3]. Optimizing and improving the quantum efficiency of this type of photocatalysis requires a detailed analysis of these complex underlying mechanisms and precise measurement of the kinetic data involved [19]. Since these photocat-

DOI: 10.1063/1674-0068/cjcp2407098

alytic reactions are typically driven by electron transfer between the catalytically active excited states of photocatalysts and RCOCOOH substrates, the quenching efficiency of this key step largely determines the quantum efficiency of the entire catalytic cycle. Therefore, it is crucial to obtain information on the properties of these catalytically active excited states, such as excited-state singlet/triplet and lifetimes, as well as their quenching rate constants by substrates. However, studies focusing on these key reaction steps and kinetic information remain scarce.

In this context, using time-resolved emission and absorption spectroscopic techniques, we thoroughly explored the initial quenching steps of various photocatalysts previously reported for photoredox catalytic RCOCOOH radical acylation reactions, including $[Ir(dFCF_3ppy)_2(dtbbpy)]^+$ (IrIII), Eosin Y (EY), Rose Bengal (RB), and 4CzPN. We found that the photocatalytic excited state of RB is its lowest triplet state: ^{3}RBH* (RBH, the protonated form of RB). The lifetimes of ^{3}RBH* are 103 ns in air and 3.4 μs under anaerobic conditions. In contrast, the photocatalytic excited states of both EY and 4CzPN are their singlet states: ^{1}EYH* (EYH, the protonated form of EY) and ^{1}4CzPN*, with measured lifetimes of 2.9 ns and 5.1 ns, respectively. Meanwhile, we measured the second-order rate constants for the quenching of the photocatalytic excited states of these catalysts by electron transfer from α-keto acids (PhCOCOOH): ^{1}EYH*, 2.3×10^9 $(mol/L)^{-1}\cdot s^{-1}$; ^{3}RBH*, 3.2×10^8 $(mol/L)^{-1}\cdot s^{-1}$; ^{1}4CzPN*, 2.8×10^8 $(mol/L)^{-1}\cdot s^{-1}$. Together with the photocatalytic excited-state properties and quenching data recently reported by our group for IrIII as the photocatalyst (^{3}IrIII*, 2.8×10^7 $(mol/L)^{-1}\cdot s^{-1}$, with lifetimes of 200 ns in air and 2.3 μs in anaerobic conditions), we obtained critical kinetic data on the substrate concentration-dependent quenching efficiencies for these four photocatalysts under both air and anaerobic conditions. Additionally, through steady-state chromatography measurements, we determined the quantum efficiencies for photocatalytic decarboxylation of α-keto acids (IrIII > RBH > EYH > 4CzPN) for these four species, and established correlations between quantum efficiencies and the initial quenching process. Based on these findings, we presented photocatalysts (IrIII/RBH) and reaction conditions (anaerobic environment) that potentially exhibit high catalytic quantum efficiency. These results provide a foundational basis for the rational design of novel photocatalytic RCOCOOH radical acylation systems with high quantum efficiency.

II. MATERIALS AND METHODS

A. Materials

$[Ir(dFCF_3ppy)_2(dtbbpy)]PF_6$ (Macklin), Rose Bengal (Aladdin), Eosin Y (Macklin), 4CzPN (APINNO), benzoylformic acid (Innochem), acetonitrile (CH_3CN, Macklin), disodium hydrogen phosphate (Na_2HPO_4, Innochem), monosodium phosphate (NaH_2PO_4, Innochem) were used as received. Ultrapure water was obtained by millipore filtration.

B. Time-resolved luminescence spectra

Time-resolved luminescence spectra were measured by the high-resolution streak camera system through the combined operation of a streak camera (C10910-05, Hamamatsu) with a CMOS camera (C13440-20CU) and a spectrometer (HRS-300-S). The 430 nm excitation light is generated by an OPA, and the fundamental pulse (800 nm, 40 fs, 1 kHz) is produced by a Ti:sapphire laser system (Coherent Astrella).

C. Laser flash photolysis

Nanosecond time-resolved transient absorption spectra were measured using a flash photolysis setup Edinburgh LP980 spectrometer (Edinburgh Instruments Ltd.). A Surelite II-10 Q-Switched Nd:YAG laser (Continuum) provides third harmonic laser pulses at 355 nm with a repetition rate of 10 Hz and maximum output of 1.5 W. The laser output was directed to a Horizon I Mid-band Optical Parametric Oscillator (OPO) (Continuum) to produce tunable pump pulses from 192 nm to 2750 nm spectral region. In this work, the sample was excited by a 430 nm laser pulse (1 Hz, 20 $mJ\cdot pulse^{-1}\cdot cm^{-2}$, FWHM ≈ 7 ns).

D. Steady-state spectral measurement

The UV-Vis absorption spectra were measured using a UV-Vis spectrometer (U-3010, Hitachi). The scan speed was 600 nm/min. Emission spectra were measured on a fluorescence spectrometer (F4600, Hitachi). 1 cm × 1 cm cuvettes were used for these measurements.

DOI: 10.1063/1674-0068/cjcp2407098

E. Steady-state photocatalytic measurement

For photocatalytic experiments, 28 μmol benzoylformic acid, 42 μmol (1.5 eq) 3-penten-2-one and 0.28 μmol (1 mol%) photocatalyst were dissolved in 0.35 mL CH_3CN, while Na_2HPO_4 and NaH_2PO_4, 26.25 μmol of each, were dissolved in 0.35 mL water. Two solutions were further mixed and sonicated to achieve a homogeneous reaction solution, which was then transferred into a sealed quartz cuvette and degassed by bubbling Ar via an needle for 60 s. The photocatalytic reactions were carried out by irradiating the sample with a 450 nm beam of around 300 mW from a CW-laser at room temperature for 40 min. The samples before and after illumination were further analyzed by a ultra-performance liquid chromatography (Shimadzu LC-20) equipped with a UV detector and a phenyl reversed phase column (Agilent Poroshell 120, 4.6×150 mm, 2.7 μm). A gradient elution program with components of acetonitrile-water mixed mobile phase varying from 3/7 to 6.5/3.5 (V/V), and total flow rate of 1 mL/min was applied.

III. RESULTS AND DISCUSSION

A. The quenching of IrIII triplet state (^{3}IrIII*) by the α-keto acid substrates

Using $[Ir(dFCF_3ppy)_2(dtbbpy)]^+$ (IrIII) as the photocatalysts, a series of important acylation reactions over the past decade have been achieved [5–7, 9, 11, 13, 14]. Due to the strong spin-orbit coupling of the Ir complex ($\xi_{Ir}=3909$ $(mol/L)^{-1}\cdot cm^{-1}$), it readily undergoes intersystem crossing (ISC) to triplet states (<100 fs, $\Phi_{ISC}=1$), thereby suppressing photochemical and photophysical processes in its singlet [20–22]. Our very recent study has clearly demonstrated that the IrIII photocatalytic α-keto acid radical acylation reaction is initiated by the electron-transfer quenching of IrIII triplet (^{3}IrIII*) with α-keto acid substrates [23]. In that work, key kinetic data were clearly measured and obtained, including the decay rate constants of ^{3}IrIII* under both air (5.0×10^6 s^{-1}) and anaerobic conditions (4.3×10^5 s^{-1}), as well as the second-order quenching reaction rate constant for α-keto acid substrates (PhCOCOOH, $k_2=2.8\times10^7$ $(mol/L)^{-1}\cdot s^{-1}$).

For photocatalytic α-keto acids radical acylation reactions involving photocatalyst triplets (^{3}PC*), the quenching efficiency of ^{3}PC* by α-keto acid substrates under both air and anaerobic conditions can be mathematically expressed through the following formulas:

$$Q^{air}_{^3PC^*}=\frac{k_2[Substrate]}{k_2\,[Substrate]+k_1^{air}}\times\Phi_{ISC} \tag{1}$$

$$Q^{anaerobic}_{^3PC^*}=\frac{k_2[Substrate]}{k_2\,[Substrate]+k_1^{anaerobic}}\times\Phi_{ISC} \tag{2}$$

Here, k_2 signifies the second-order quenching reaction rate constant of ^{3}PC* by α-keto acid substrates. k_1^{air} and $k_1^{N_2}$ represent the self-decay rate constant for ^{3}PC* under air and anaerobic (*e.g.* N_2-saturated) conditions, respectively. [Substrate] is the concentration of α-keto acid substrates used in the quenching reaction, and Φ_{ISC} is the quantum yield of intersystem crossing for ^{3}PC*.

Based on the above expressions, together with the collected kinetic information for ^{3}IrIII*, including the decay rate constants of ^{3}IrIII* ($k_1^{air}=5.0\times10^6$ s^{-1} and $k_1^{N_2}=4.3\times10^5$ s^{-1}), ^{3}IrIII* quantum yield ($\Phi_{ISC}=1$), and the second-order quenching reaction rate constant by α-keto acid substrates (PhCOCOOH, $k_2=2.8\times10^7$ $(mol/L)^{-1}\cdot s^{-1}$), the concentration-dependent quantum quenching efficiency of ^{3}IrIII* by α-keto acid substrates (PhCOCOOH) under both air ($Q^{air}_{^3IrIII^*}$) and anaerobic ($Q^{anaerobic}_{^3IrIII^*}$) conditions, can thus be obtained, respectively.

$$\begin{aligned}Q^{air}_{^3IrIII^*}&=\frac{k_2[PhCOCOOH]}{k_2[PhCOCOOH]+k_1^{air}}\times\Phi_{ISC}\\&=\frac{2.8\times10^7\times[PhCOCOOH]}{2.8\times10^7\times[PhCOCOOH]+5.0\times10^6}\end{aligned} \tag{3}$$

$$\begin{aligned}Q^{anaerobic}_{^3IrIII^*}&=\frac{k_2[PhCOCOOH]}{k_2[PhCOCOOH]+k_1^{anaerobic}}\times\Phi_{ISC}\\&=\frac{2.8\times10^7\times[PhCOCOOH]}{2.8\times10^7\times[PhCOCOOH]+4.3\times10^5}\end{aligned} \tag{4}$$

Based on the derived expressions (3) and (4), we further plotted the relationship curves between the quantum quenching efficiency of ^{3}IrIII* by PhCOCOOH and the concentration of PhCOCOOH under both air and anaerobic conditions. As shown in FIG. 1, the quantum quenching efficiency ($Q^{air}_{^3IrIII^*}/Q^{anaerobic}_{^3IrIII^*}$) increases with the increasing concentration of PhCOCOOH in both

DOI: 10.1063/1674-0068/cjcp2407098

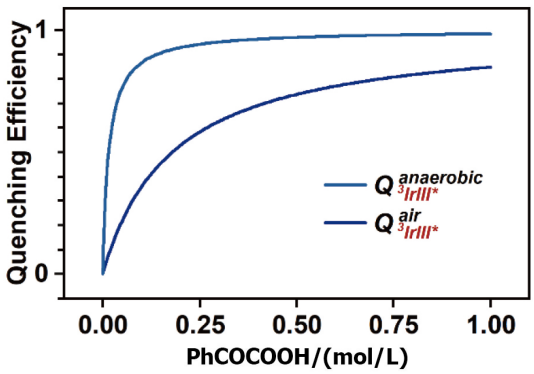

FIG. 1 The quenching efficiency of ^{3}IrIII* at different concentrations of PhCOCOOH in both air and anaerobic conditions.

conditions. Additionally, the quantum quenching efficiency is consistently higher under anaerobic condition than under air condition. This is because, in the presence of air, oxygen introduces an additional quenching pathway for ^{3}IrIII*, competing with PhCOCOOH and reducing its corresponding quantum quenching efficiency. Moreover, under anaerobic conditions, if the concentration of PhCOCOOH is sufficiently high (*e.g.* 1 mol/L), the quantum efficiency of the ^{3}IrIII* quenching pathway by PhCOCOOH can approach near unity ([PhCOCOOH] = 1 mol/L, $Q_{^3\mathrm{IrIII}^*}^{\mathrm{anaerobic}} = 0.985$). This high quantum quenching efficiency of ^{3}IrIII* by PhCOCOOH suggests that IrIII could potentially be one of the most effective photocatalysts for catalyzing α-keto acids radical acylation reactions.

B. The quenching of protonated Eosin Y singlet state (^{1}EYH*) by the α-keto acid substrates

Besides these heavy metal complexes as photocatalysts, various organic dyes have also been utilized to promote the efficient photoinduced conversion of substrates into desired products, as they are low-cost and readily available [24, 25]. Among these organic dyes, Eosin Y, a member of the triarylmethane dyes, has been shown to facilitate radical acylation reactions of α-keto acids [8].

When in solution, due to the presence of two relatively acidic protons ($pK_{a1} = 2.0$ and $pK_{a2} = 3.8$ in water), Eosin Y generally exists in two distinct forms in solution: an anionic form (denoted as EY) and a protonated form (denoted as EYH), as depicted in Scheme 1 [26, 27]. These two forms are pH dependent: at low H^+ concentrations (*e.g.* pH > 5), Eosin Y predominantly exists in its anionic EY form, whereas at high H^+ concentrations (*e.g.* pH < 1), the -O^-/COO^- groups transform into -OH/COOH, resulting in the protonated EYH form [27]. Given the potential differences in the properties of the singlet and triplet states between these two forms, we conducted individual investigations into their excited-state characteristics and their reaction with α-keto acids in the following experiments.

1. The anionic form of Eosin Y (EY) is not the catalytically active form

As shown in FIG. 2(a), the steady-state UV-Vis absorption spectrum of EY displays broad absorptions around both 300–400 nm and 450–550 nm, with a peak at 520 nm, consistent with previous reports. The steady-state absorption spectrum of the mixed solution containing EY and α-keto acid (PhCOCOOH) matches the combined spectra of the individual components, confirming the absence of any chemical reaction between EY and α-keto acid.

First, fluorescence quenching experiments were conducted to evaluate the potential reaction between the singlet state of EY (^{1}EY*) and α-keto acid substrates (PhCOCOOH). As shown in FIG. 2(b), the steady-state fluorescence spectrum of EY exhibits a strong band peaking at 550 nm. In the presence of α-keto acids (PhCOCOOH), the emission intensity of ^{1}EY* remains unchanged, indicating no reaction between ^{1}EY* and α-keto acid substrates (PhCOCOOH). This excludes the possibility of ^{1}EY* as the catalytically active state for facilitating radical acylation reactions of α-keto acids.

Second, employing nanosecond time-resolved absorption spectroscopy, we further assessed the possible reaction between the triplet state of EY (^{3}EY*) and PhCOCOOH. Upon 532 nm laser excitation of EY under N_2-saturated condition, as shown in FIG. 2(c), both ground-state bleaching (470 – 560 nm, negative peaking around 520 nm) and excited-state absorption of ^{3}EY* (350–470 nm and 550–700 nm) are initially observed. The decay dynamics of ^{3}EY* were monitored at 580 nm. FIG. 2(d) displays the decay curves for ^{3}EY* under both N_2-saturated and air conditions. The decay of ^{3}EY* at 580 nm follows a monoexponential behavior, with a lifetime of 25 μs ($k_1^{N_2} = 4.0 \times 10^4$ s^{-1}) under N_2-saturated condition and a lifetime of 240 ns ($k_1^{\mathrm{air}} = 4.2 \times 10^6$ s^{-1}) under air condition. This pronounced oxygen sensitivity further supports the assignment of this excited state as ^{3}EY*. In the presence of PhCOCOOH (FIG. 2(d)), the decay dynamics of ^{3}EY* also remains unchanged, indi-

DOI: 10.1063/1674-0068/cjcp2407098

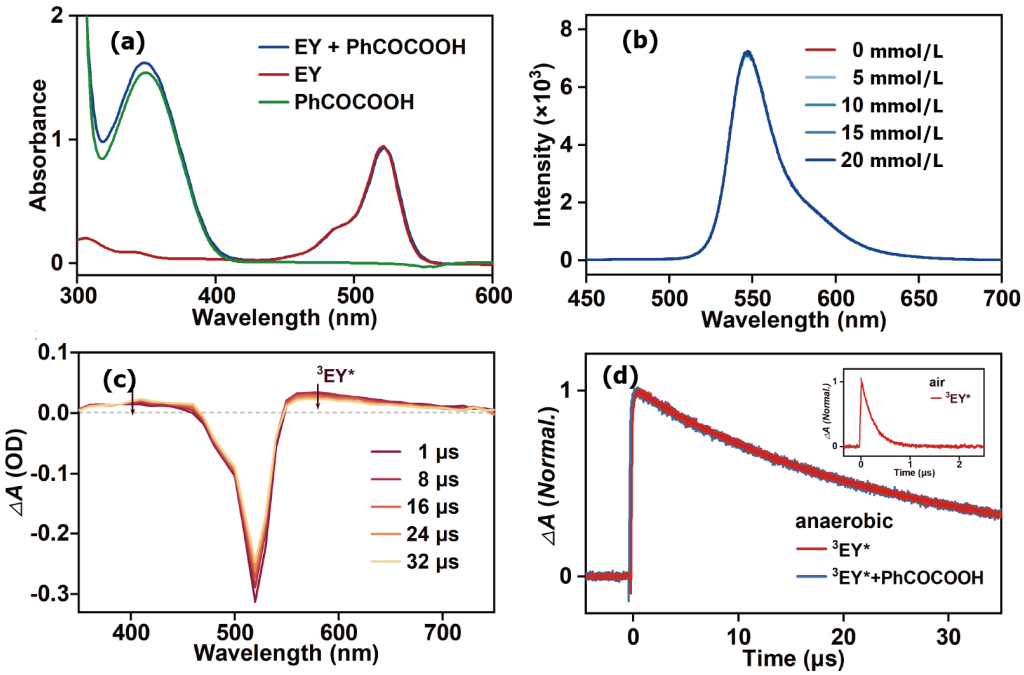

FIG. 2 (a) Steady-state UV-Vis absorption spectra for 10 μmol/L EY (red), 20 mmol/L PhCOCOOH (green) and 10 μmol/L EY+20 mmol/L PhCOCOOH (blue) in ACN/phosphate buffer (pH=7.0); (b) steady-state emission spectra of EY (10 μmol/L) at different concentrations of PhCOCOOH following 532 nm excitation; (c) transient absorption spectra of EY (10 μmol/L) under deoxygenated condition; (d) in the presence of PhCOCOOH, the decay dynamics of ^{3}EY* at 580 nm under N_2-saturated and air conditions (inset).

cating no reaction between ^{3}EY* and α-keto acid substrates (PhCOCOOH). This further excludes the possibility of ^{3}EY* as the catalytically active state for facilitating radical acylation reactions of α-keto acids. Taken together, our results here clearly demonstrate that the anionic Eosin Y (EY) should not be the catalytically active form.

2. The singlet state of protonated Eosin Y (^{1}EYH*) is the catalytically active species

As shown in FIG. 3(a), the steady-state UV-Vis absorption spectrum of the protonated Eosin Y (EYH) displays broad absorptions spanning from 400 nm to 550 nm, with two resolved bands around 480 and 510 nm. Similarly, the steady-state absorption spectrum of the mixed solution containing EYH and α-keto acid (PhCOCOOH) matches the combined spectra of the individual components, confirming the absence of any chemical reaction between EYH and α-keto acid.

Then, fluorescence quenching experiments were conducted to evaluate the potential reaction between the singlet state of EYH (^{1}EYH*) and α-keto acid substrates (PhCOCOOH). As shown in FIG. 3(b), the steady-state fluorescence spectrum of EYH exhibits a strong band peaking at 560 nm. In the presence of α-keto acids (PhCOCOOH), the emission intensity of ^{1}EYH* is noticeably reduced, exhibiting a linear concentration dependence. This results clearly demonstrate that ^{1}EYH* can be efficiently quenched by α-keto acids (PhCOCOOH) substrates. Meanwhile, for the time-resolved emission of ^{1}EYH*, as shown in FIG. 3(c), the decay of ^{1}EYH* follows in a mono-exponential behavior with a lifetime of 2.9 ns ($k_1 = 3.4 \times 10^8$ s^{-1}). Interestingly, in the presence of excess α-keto acids (PhCOCOOH) substrates, the decay of ^{1}EYH* is significantly different, showing an accelerated decay at higher concentration of substrates. Linear fitting of the measured pseudo-first-order reaction rate constants *vs.* PhCOCOOH concentration enables direct determination for the quenching second-order reaction rate constant (1.1×10^9 (mol/L)$^{-1}$·s^{-1}, FIG. 3(d)) of ^{1}EYH* by PhCOCOOH.

Subsequently, employing nanosecond time-resolved absorption spectroscopy, we further assessed the possible reaction between the triplet state of EYH (^{3}EYH*) and PhCOCOOH. Upon 532 nm laser excitation of EYH under N_2-saturated condition, as shown in FIG. 3(e), both ground-state bleaching (350–550 nm, two resolved negative bands around 480 and 510 nm) and excited-state absorption of ^{3}EYH* (300–350 nm,

DOI: 10.1063/1674-0068/cjcp2407098

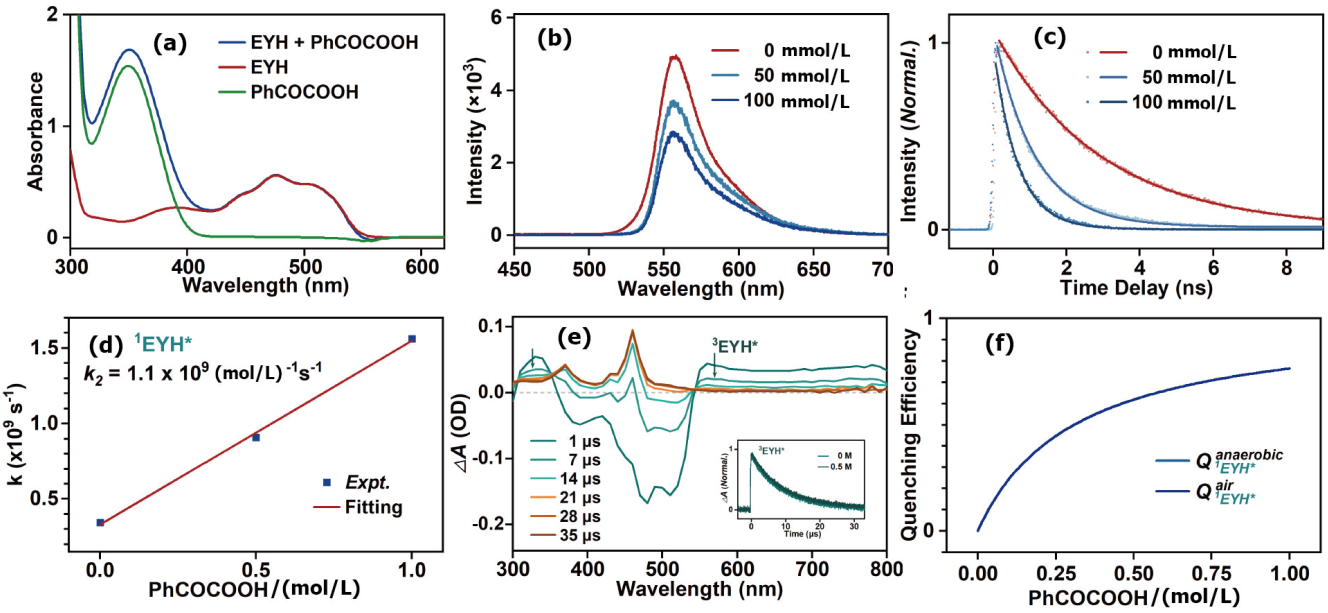

FIG. 3 (a) Steady-state UV-Vis absorption spectra for EYH, with 300 μmol/L EY (red), 20 mmol/L PhCOCOOH (green) and 300 μmol/L EY+20 mmol/L PhCOCOOH (blue) in ACN/phosphate buffer (pH=1.0); (b) steady-state emission spectra for EYH, with EY (300 μmol/L) at different concentrations of PhCOCOOH following 532 nm excitation; (c) normalized transient emission kinetics of ^{1}EYH* at different concentrations of PhCOCOOH following 532 nm excitation; (d) Stern-Volmer plot obtained from the decay lifetime of ^{1}EYH* with different concentrations of PhCOCOOH; (e) transient absorption spectra of EYH (300 μmol/L) under deoxygenated condition; in the presence of PhCOCOOH, the decay dynamics of ^{3}EYH* at 570 nm under N_2-saturated condition (inset); (f) the quenching efficiency of ^{1}EYH* at different concentrations of PhCOCOOH.

peaking around 330 nm and featureless flat absorption within 550–800 nm) are initially observed. The decay dynamics of ^{3}EYH* were monitored at 570 nm. Inset in FIG. 3(e) displays the decay curves for ^{3}EYH* in the absence and in the presence of PhCOCOOH, showing the decay dynamics of ^{3}EYH* unaffected by α-keto acids substrates. This kinetics analysis rules out the possibility of ^{3}EYH* as the catalytically active species triggering the conversion of α-keto acids into acylation radicals.

On the basis of above accumulated evidence, we deduce that for Eosin Y, only the singlet state of protonated Eosin Y (^{1}EYH*) is the catalytically active species that promotes conversion of α-keto acids into acylation radicals. We note that besides the form of Eosin Y being affected by pH, the form of the substrate PhCOCOOH is also influenced. At low pH, it exists as PhCOCOOH, but at high pH, PhCOCOOH is expected to easily deprotonate and exist in the deprotonated form $PhCOCOO^-$. Compared to the PhCOCOOH form, the $PhCOCOO^-$ form, due to its higher electron density, is theoretically more prone to donate electrons, making it more likely to quench the excited state. However, we found that under neutral conditions, EY exists in its anionic form and the substrate exists as $PhCOCOO^-$, but no effective quenching occurs. This indicates that the effect of pH on the form of the photocatalyst and its excited state activity is more significant than the change in the form of the substrate.

3. The quenching efficiency of ^{1}EYH* by α-keto acid substrates

For photocatalytic α-keto acids radical acylation reactions involving photocatalyst singlets (^{1}PC*), the quenching efficiency of ^{1}PC* by α-keto acid substrates can be mathematically expressed through the following formulas:

$$Q^{\text{air}}_{^1\text{PC}^*}=Q^{\text{anaerobic}}_{^1\text{PC}^*}=\frac{k_2[\text{Substrate}]}{k_2\,[\text{Substrate}]+k_1} \tag{5}$$

Here, k_2 signifies the second-order quenching reaction rate constant of ^{1}PC* by α-keto acid substrates. k_1 represents the self-decay rate constant for ^{1}PC*. [Substrate] is the concentration of α-keto acid substrates used in the quenching reaction. Considering that the singlet state is not affected by oxygen concentration, the quenching efficiency under both air and anaerobic conditions can be expressed using the same equation.

Based on the above expression, together with the col-

DOI: 10.1063/1674-0068/cjcp2407098

TABLE I Quenching quantum efficiency of photocatalysts (^{3}IrIII*, ^{1}EYH*, ^{3}RBH*, and ^{1}4CzPN*) with low, medium, and high concentrations of α-keto acids (PhCOCOOH).

[PhCOCOOH]/(mol/L)	^{3}IrIII*		^{1}EYH*		^{3}RBH*		^{1}4CzPN*	
	Q_{air}	$Q_{anaerobic}$	Q_{air}	$Q_{anaerobic}$	Q_{air}	$Q_{anaerobic}$	Q_{air}	$Q_{anaerobic}$
0.01	5.3%	39.4%	3.1%	3.1%	19.1%	70.6%	1.4%	1.4%
0.1	35.9%	86.7%	24.4%	24.4%	59.1%	76.3%	12.3%	12.3%
1	84.8%	98.5%	76.4%	76.4%	74.7%	76.9%	58.3%	58.3%

lected kinetic information for EYH, including the decay rate constants of ^{1}EYH* ($k_1 = 3.4\times10^8$ s^{-1}) and the second-order quenching reaction rate constant by α-keto acid substrates (PhCOCOOH, $k_2 = 1.1\times10^9$ (mol/L)$^{-1}\cdot$s^{-1}), the concentration-dependent quantum quenching efficiency of ^{1}EYH* by α-keto acid substrates (PhCOCOOH) can thus be obtained (Eq.(6)).

$$Q_{^1PC^*}^{air} = Q_{^1PC^*}^{anaerobic} = \frac{1.1\times10^9\times[PhCOCOOH]}{1.1\times10^9\times[PhCOCOOH] + 3.4\times10^8} \quad (6)$$

Based on the derived expressions (6), we further plotted the relationship curves between the quantum quenching efficiency of ^{1}EYH* by PhCOCOOH and the concentration of PhCOCOOH. As shown in FIG. 3(f), the quantum quenching efficiency increases with the increasing concentration of PhCOCOOH. Besides, we found that the quenching efficiencies of ^{1}EYH* at low (0.01 mol/L, $Q = 3.1\%$), medium (0.1 mol/L, $Q = 24.4\%$), and high (1 mol/L, $Q = 76.4\%$) PhCOCOOH substrate concentrations are consistently lower than those of ^{3}IrIII* under both aerobic and anaerobic conditions (0.01 mol/L, $Q_{air} = 5.3\%$, $Q_{anaerobic} = 39.4\%$; 0.1 mol/L, $Q_{air} = 35.9\%$, $Q_{anaerobic} = 86.7\%$; 1 mol/L, $Q_{air} = 84.8\%$, $Q_{anaerobic} = 98.5\%$) (Table I), even though the bimolecular quenching rate constant of ^{1}EYH* by PhCOCOOH (1.1×10^9 (mol/L)$^{-1}\cdot$s^{-1}) is significantly higher than that of ^{3}IrIII* (2.8×10^7 (mol/L)$^{-1}\cdot$s^{-1}). This can be attributed to the fact that quenching efficiency depends not only on the bimolecular quenching rate constant but also on the intrinsic decay rate constant of photocatalytically active excited state. The lower the intrinsic decay rate constant, the more favorable it is for the bimolecular reaction to dominate the decay pathway of the photocatalytically active excited state, thereby enhancing the quenching efficiency. Compared to the decay rate constant of ^{1}EYH* (3.4×10^8 s^{-1}), we found that the decay rate constant of ^{3}IrIII* is significantly lower under both aerobic (5.0×10^6 s^{-1}) and anaerobic (4.3×10^5 s^{-1}) conditions. This explains why ^{3}IrIII* exhibits higher quenching efficiency at the same substrate concentration. These results highlight the importance of considering both factors when evaluating the overall efficiency of a quenching reaction, as relying solely on the bimolecular quenching rate constant provides an incomplete assessment of reaction efficiency.

C. The quenching of protonated Rose Bengal triplet (^{3}RBH*) by the α-keto acid substrates

Rose Bengal, a common organic photocatalyst, has a xanthene backbone and features aromatic ring structures similar to those of Eosin Y [13, 28]. However, due to differences in their specific substituents, Rose Bengal is primarily substituted with iodine while Eosin Y is substituted with bromine (Scheme 1), and their chemical properties and applications, such as their use as the photocatalysts for facilitating the radical acylation of α-keto acids, may be accordingly impacted.

Likely, in solution, due to the presence of two relatively acidic protons ($pK_{a1} = 1.9$ and $pK_{a2} = 3.9$ in water), Rose Bengal generally exists in two distinct forms in solution: an anionic form (denoted as RB) and a protonated form (denoted as RBH), as depicted in Scheme 1 [27]. At high pH (*e.g.* pH > 5), Rose Bengal predominantly exists in its anionic RB form, whereas at low pH (*e.g.* pH < 1), the protonated RBH form become predominant [27]. Given the potential differences in the properties of the singlet and triplet states between these two forms, we conducted individual investigations into their excited-state characteristics and their reaction with α-keto acids in the following experiments.

1. The anionic form of Rose Bengal (RB) is not the catalytically active form

As shown in FIG. 4(a), the steady-state UV-Vis absorption spectrum of RB is very similar in shape to that of EY, but its maximum absorption peak is red-shifted

DOI: 10.1063/1674-0068/cjcp2407098

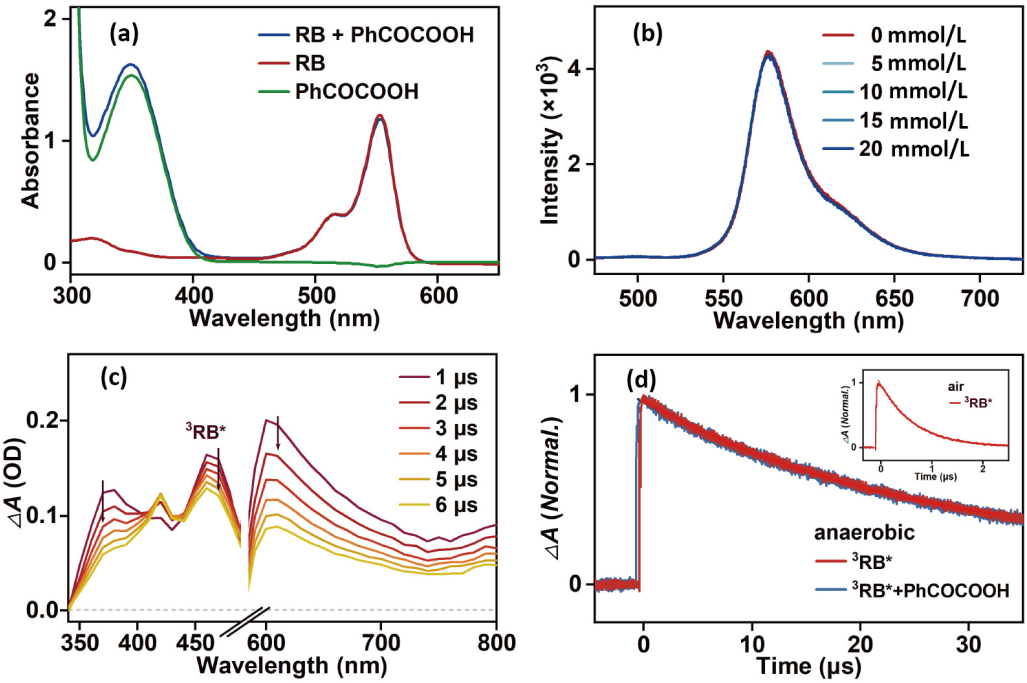

FIG. 4 (a) Steady-state UV-Vis absorption spectra for 10 μmol/L RB (red), 20 mmol/L PhCOCOOH (green) and 10 μmol/L RB+20 mmol/L PhCOCOOH (blue) in ACN/phosphate buffer (pH=7.0); (b) steady-state emission spectra of RB (10 μmol/L) at different concentrations of PhCOCOOH following 532 nm excitation; (c) transient absorption spectra of RB (10 μmol/L) under deoxygenated condition; (d) in the presence of PhCOCOOH, the decay dynamics of ^{3}RB* at 610 nm under N_2-saturated and air conditions (inset).

from 520 nm (as seen in EY) to 550 nm. Similarly, we found that the absorption spectrum of the mixed solution (RB+PhCOCOOH) is the sum of the individual spectra of the two species, ruling out the possibility of their reaction in the ground state. Then, we performed steady-state fluorescence quenching experiments and found that the emission intensity of ^{1}RB* (peaking around 580 nm) remains unchanged in the presence of varying concentrations of α-keto acids (PhCOCOOH) (FIG. 4(b)). This excludes the possibility of ^{1}RB* being the catalytically active state for facilitating radical acylation reactions of α-keto acids.

Subsequently, using nanosecond time-resolved absorption spectroscopy, we investigated the potential quenching reaction of the triplet state of RB (^{3}RB*) by PhCOCOOH. Upon 532 nm laser excitation of RB under N_2-saturated condition, a broad excited-state absorption of ^{3}RB* (350–700 nm) featuring three characteristic bands around 370, 470, and 610 nm, is initially observed, as shown in FIG. 4(c). The decay dynamics of ^{3}RB* were monitored at 610 nm. FIG. 4(d) shows the decay curves for ^{3}RB*, which exhibits an accelerated decay under air compared to N_2-saturated conditions. This pronounced oxygen sensitivity further supports the assignment of this transient as ^{3}RB*. In the presence of PhCOCOOH (FIG. 4(d)), the decay dynamics of ^{3}RB* keep unchanged, indicating no reaction between ^{3}RB* and α-keto acid substrates (PhCOCOOH). This further excludes the possibility of ^{3}RB* being the catalytically active state for facilitating radical acylation reactions of α-keto acids. Overall, our results clearly demonstrate that the anionic Rose Bengal (RB) is not the catalytically active form.

2. The triplet state of protonated Rose Bengal (^{3}RBH*) is the catalytically active species

As shown in FIG. 5(a), the steady-state UV-Vis absorption spectrum of the protonated Rose Bengal (RBH) displays broad absorptions spanning from 400 nm to 550 nm, with two resolved bands around 500 and 560 nm. Similarly, the steady-state absorption spectrum of the mixed solution containing RBH and α-keto acid (PhCOCOOH) matches the combined spectra of the individual components, confirming the absence of any chemical reaction between RBH and α-keto acid. Then, fluorescence quenching experiments were conducted to evaluate the potential reaction between the singlet state of RBH (^{1}RBH*) and α-keto acid substrates (PhCOCOOH). As shown in FIG. 5(b), the

DOI: 10.1063/1674-0068/cjcp2407098

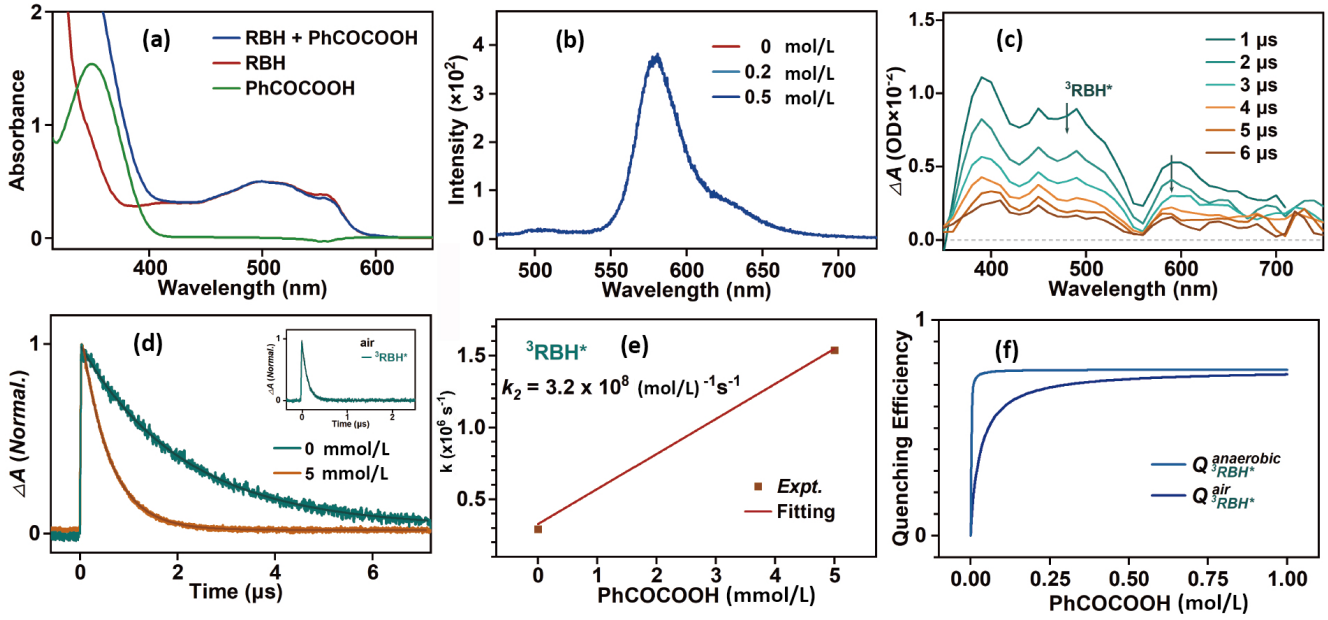

FIG. 5 (a) Steady-state UV-Vis absorption spectra for RBH, with 300 μmol/L RB (red), 20 mmol/L PhCOCOOH (green) and 300 μmol/L RB+20 mmol/L PhCOCOOH (blue) in ACN/phosphate buffer (pH 1.0); (b) steady-state emission spectra for RBH, with RB (300 μmol/L) at different concentrations of PhCOCOOH following 532 nm excitation; (c) transient absorption spectra of RBH (300 μmol/L) under deoxygenated condition; (d) in the presence of PhCOCOOH, the normalized decay dynamics of ^{3}RBH* at 480 nm under N_2-saturated condition and air conditions (inset); (e) Stern-Volmer plot obtained from the decay lifetime of ^{3}RBH* with different concentrations of PhCOCOOH; (f) the quenching efficiency of ^{3}RBH* at different concentrations of PhCOCOOH.

steady-state fluorescence spectrum of RBH exhibits a strong band peaking at 580 nm. In the presence of α-keto acids (PhCOCOOH), the emission intensity of ^{1}RBH* remains unchanged, indicating no reaction between ^{1}RBH* and α-keto acid substrates (PhCOCOOH). This excludes the possibility of ^{1}RBH* as the catalytically active state for facilitating radical acylation reactions of α-keto acids.

Subsequently, employing nanosecond time-resolved absorption spectroscopy, we further assessed the possible reaction between the triplet state of RBH (^{3}RBH*) and PhCOCOOH. Upon 532 nm laser excitation of RBH under N_2-saturated condition, as shown in FIG. 5(c), a broad excited-state absorption of ^{3}RBH* spanning from 400 nm to 700 nm (two bands around 480 nm and 590 nm) is initially observed. The decay dynamics of ^{3}RBH* were monitored at 480 nm. FIG. 5(d) displays the decay curves for ^{3}RBH* under both N_2-saturated and air conditions. The decay of ^{3}RBH* follows a monoexponential behavior, with a lifetime of 3.4 μs ($k_1^{N_2} = 2.9\times10^5$ s^{-1}) under N_2-saturated condition and a lifetime of 103 ns ($k_1^{air} = 9.7\times10^6$ s^{-1}) under air condition. This pronounced oxygen sensitivity further supports the assignment of this excited state as ^{3}RBH*. Interestingly, under N_2-saturated condition, the decay of ^{3}RBH* is significantly accelerated decay in the presence of PhCOCOOH (FIG. 5(d)). Linear fitting of the measured pseudo-first-order reaction rate constants *vs.* PhCOCOOH concentration enables direct determination for the quenching second-order reaction rate constant (3.2×10^8 (mol/L)$^{-1}\cdot$s^{-1}, FIG. 5(e)) of ^{3}RBH* by PhCOCOOH.

On the basis of above accumulated evidence, we deduce that for Rose Bengal, only the triplet state of protonated Rose Bengal (^{3}RBH*) is the catalytically active species that promotes conversion of α-keto acids into acylation radicals.

3. The quenching efficiency of ^{3}RBH* by α-keto acid substrates

Based on expressions of Eq.(1) and Eq.(2), together with the collected kinetic information for RBH, the decay rate constants of ^{3}RBH* ($k_1^{air} = 9.7\times10^6$ s^{-1} and $k_1^{N_2} = 2.9\times10^5$ s^{-1}), ^{3}RBH* quantum yield ($\Phi_{ISC} = 0.77$) [3, 29, 30], and the second-order quenching reaction rate constant by α-keto acid substrates (PhCOCOOH, $k_2 = 3.2\times10^8$ (mol/L)$^{-1}\cdot$s^{-1}), the concentration-dependent quantum quenching efficiency of ^{3}RBH* by α-keto acid substrates (PhCOCOOH) under

DOI: 10.1063/1674-0068/cjcp2407098

both air ($Q^{\text{air}}_{^3\text{RBH}^*}$) and anaerobic ($Q^{\text{anaerobic}}_{^3\text{RBH}^*}$) conditions, can thus be obtained, respectively.

$$Q^{\text{air}}_{^3\text{RBH}^*} = \frac{k_2[\text{PhCOCOOH}]}{k_2\,[\text{PhCOCOOH}] + k_1^{\text{air}}} \times \Phi_{\text{ISC}} = \frac{3.2\times10^8\times[\text{PhCOCOOH}]}{3.2\times10^8\times[\text{PhCOCOOH}] + 9.7\times10^6} \times 0.77 \tag{7}$$

$$Q^{\text{anaerobic}}_{^3\text{RBH}^*} = \frac{k_2[\text{PhCOCOOH}]}{k_2[\text{PhCOCOOH}] + k_1^{\text{anaerobic}}} \times \Phi_{\text{ISC}} = \frac{3.2\times10^8\times[\text{PhCOCOOH}]}{3.2\times10^8\times[\text{PhCOCOOH}] + 2.9\times10^5} \times 0.77 \tag{8}$$

Based on the derived Eqs. (7) and (8), we further plotted the relationship curves between the quantum quenching efficiency of ^{3}RBH* by PhCOCOOH and the concentration of PhCOCOOH under both air and anaerobic conditions (FIG. 5(f), 0.01 mol/L, $Q_{\text{air}} = 19.1\%$, $Q_{\text{anaerobic}} = 70.6\%$; 0.1 mol/L, $Q_{\text{air}} = 59.1\%$, $Q_{\text{anaerobic}} = 76.3\%$; 1 mol/L, $Q_{\text{air}} = 74.7\%$, $Q_{\text{anaerobic}} = 76.9\%$). As shown in Table I, we found that at low concentrations of the substrate PhCOCOOH, the quenching efficiency of ^{3}RBH* surpasses that of ^{3}IrIII* under both aerobic and anaerobic conditions. However, as the concentration of PhCOCOOH increases, although the quenching efficiencies of both photocatalysts improve, the quenching efficiency of ^{3}IrIII* eventually exceeds that of ^{3}RBH*, particularly under anaerobic conditions. This observation can be attributed to the fact that quenching efficiency is determined not only by the quenching second-order reaction rate constant and the decay rate constant of the excited state, but also by the quantum yield of the catalytically active excited state of the photocatalyst. At low concentrations, the predominant factors are the second-order reaction rate constant of quenching and the decay rate constant of the excited state. In contrast, at high concentrations, the quantum yield of the catalytically active excited state becomes the primary influencing factor.

D. The quenching of 4CzPN singlet (^{1}4CzPN*) by the α-keto acid substrates

1. The singlet state of 4CzPN (^{1}4CzPN*) is the catalytically active species

4CzPN belongs to the carbazolyl benzonitriles family. The structure of 4CzPN is shown in Scheme 1, where the carbazolyl groups are positioned adjacent and opposite to the nitrile groups [31, 32]. The UV-Vis absorption spectrum is also illustrated in FIG. 6(a), highlighting the characteristic absorption bands in the UV region around 320 nm, 330 nm, and 360 nm, along with a red tail extending up to 500 nm. In like manner, the interaction between 4CzPN and α-keto acid prior to irradiation is ruled out, as the steady-state absorption spectrum of the mixed solution containing 4CzPN and α-keto acid (PhCOCOOH) matches the combined spectra of the individual components.

The steady-state fluorescence spectrum of ^{1}4CzPN* shows strong emission between 450 and 750 nm, with a peak at 600 nm (FIG. 6(b)). In the presence of PhCOCOOH, the emission intensity of ^{1}4CzPN* exhibits a slight but clear linear decrease with increasing concentration. Meanwhile, the time-resolved emission spectra of ^{1}4CzPN* exhibit a mono-exponential decay behavior (FIG. 6(c)). Through mono-exponential fitting, the decay rate constants of ^{1}4CzPN* can be determined ($k_1 = 2.0\times10^8$ s^{-1}). Furthermore, the decay of ^{1}4CzPN* is found to be accelerated in the presence of excess PhCOCOOH. Linear fitting of the measured pseudo-first-order reaction rate constants *vs.* PhCOCOOH concentration enables direct determination of the quenching second-order rate constant of ^{1}4CzPN* by PhCOCOOH (2.0×10^8 (mol/L)$^{-1}\cdot$s^{-1}, FIG. 6(d)).

Additionally, we further investigated the potential reaction between the triplet state of 4CzPN (^{3}4CzPN*) and PhCOCOOH using nanosecond time-resolved absorption spectroscopy (FIG. 6(e)). By exclusively exciting 4CzPN, we did not observe a distinct signal of ^{3}4CzPN* in the transient absorption spectra. This might be due to the relatively low quantum yield of ^{3}4CzPN* in ACN solvent. Therefore, under the conditions of ACN solvent, we excluded the contribution of ^{3}4CzPN* pathway. Thus, we conclude that for 4CzPN, the singlet state of 4CzPN (^{1}4CzPN*) should be mainly the catalytically active species that promotes conversion of α-keto acids into acylation radicals.

2. The quenching efficiency of ^{1}4CzPN* by α-keto acid substrates

Based on the expression of (5), together with the collected kinetic information for ^{1}4CzPN*, including the decay rate constants of ^{1}4CzPN* ($k_1 = 2.0\times10^8$ s^{-1}) and the second-order quenching reaction rate constant by α-

DOI: 10.1063/1674-0068/cjcp2407098

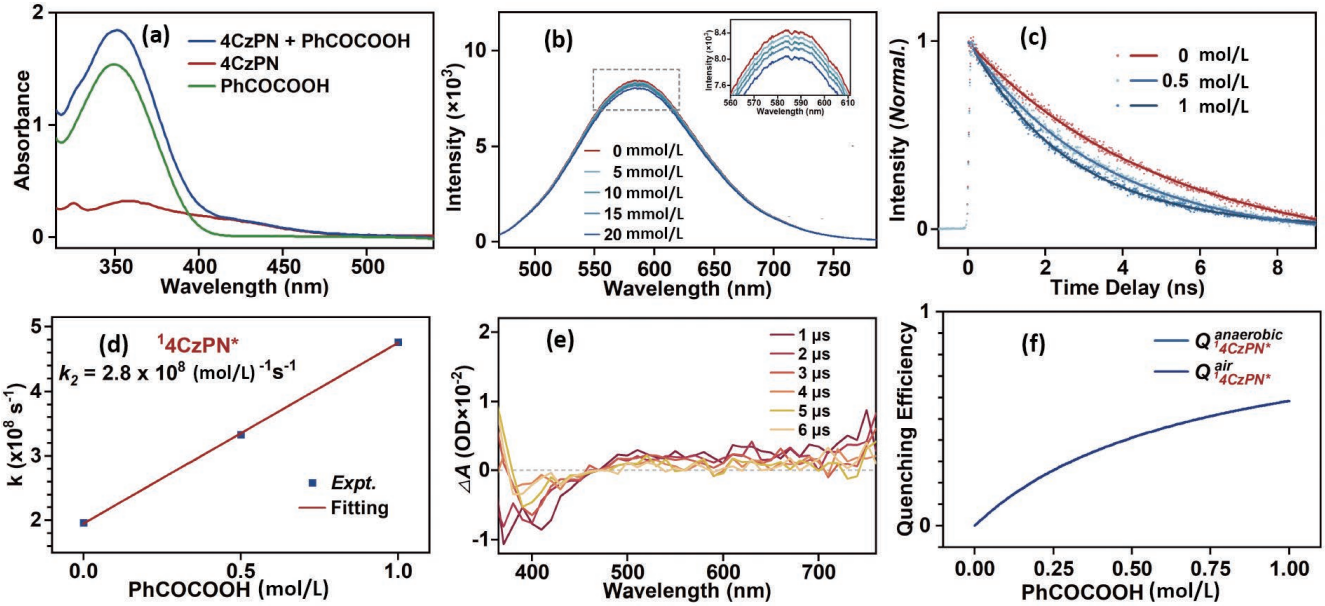

FIG. 6 (a) Steady-state UV-Vis absorption spectra for 50 μmol/L 4CzPN (red), 20 mmol/L PhCOCOOH (green) and 50 μmol/L 4CzPN+20 mmol/L PhCOCOOH (blue) in ACN; (b) steady-state emission spectra of 4CzPN (50 μmol/L) at different concentrations of PhCOCOOH following 430 nm excitation; (c) normalized transient emission kinetics of ^{1}4CzPN* at different concentrations of PhCOCOOH following 430 nm excitation; (d) Stern-Volmer plot obtained from the decay lifetime of ^{1}4CzPN* with different concentrations of PhCOCOOH; (e) transient absorption spectra of 4CzPN (50 μmol/L) under deoxygenated condition; (f) the quenching efficiency of ^{1}4CzPN* at different concentrations of PhCOCOOH.

keto acid substrates (PhCOCOOH, $k_2 = 2.8 \times 10^8$ $(\text{mol/L})^{-1} \cdot \text{s}^{-1}$), the concentration-dependent quantum quenching efficiency of ^{1}4CzPN* by α-keto acid substrates (PhCOCOOH) can thus be obtained (Eq.(9)).

$$Q^{\text{air}}_{^1\text{4CzPN*}} = Q^{\text{anaerobic}}_{^1\text{4CzPN*}} = \frac{2.8\times10^8\times[\text{PhCOCOOH}]}{2.8\times10^8\times[\text{PhCOCOOH}]+2.0\times10^8} \quad (9)$$

Based on the derived expressions (9), we further plotted the relationship curves between the quantum quenching efficiency of ^{1}4CzPN* by PhCOCOOH and the concentration of PhCOCOOH (FIG. 6(f)). Compared to the substrate concentration-dependent singlet quenching efficiency of ^{1}EYH* by PhCOCOOH, we found that the quenching efficiency of ^{1}4CzPN* is significantly lower. This discrepancy may be attributed to the considerably smaller second-order reaction rate constant of 4CzPN, despite its intrinsic singlet state lifetime being longer than that of EYH. Consequently, the quenching quantum efficiency of ^{1}4CzPN* remains much lower than that of ^{1}EYH* across low, medium, and high substrate concentrations (0.01 mol/L, $Q = 1.4\%$; 0.1 mol/L, $Q = 12.3\%$; 1 mol/L, $Q = 58.3\%$).

Furthermore, by comparing the quenching efficiencies of ^{1}EYH* and ^{1}4CzPN* with those of ^{3}IrIII* and ^{3}RBH* (Table I), we found that, overall, the quenching efficiencies of photocatalysts following the singlet state pathway are inferior to those following the triplet state pathway. This is largely due to the significantly shorter intrinsic lifetimes of singlet states compared to triplet states, resulting in higher utilization efficiencies for triplet states. Therefore, for the four representative photocatalysts mentioned above, ^{3}IrIII* and ^{3}RBH* are more effective in triggering the decarboxylation reaction of α-keto acids. Moreover, higher quenching efficiencies are always achieved under anaerobic conditions compared to aerobic conditions.

E. Steady-state photocatalysis

Steady-state photocatalytic experiments were further performed to evaluate the overall efficiency of the four photocatalysts, including $[\text{Ir}(\text{dFCF}_3\text{ppy})_2(\text{dtbbpy})]^+$, Eosin Y, Rose Bengal and 4CzPN, in photocatalytic organic transformation of α-keto acid at room temperature. The study involved conducting photocatalytic reactions between model compounds, PhCOCOOH (**1a**) and 3-penten-2-one (**2a**), in a de-aerated quartz cuvette under illumination of a 450 nm monochromatic CW-laser with light power of around 300 mW, as shown in Scheme 2. For all the photocatalytic reactions, only the acylation product (2-

DOI: 10.1063/1674-0068/cjcp2407098

Scheme 2. Photocatalytic reaction between PhCOCOOH (**1a**) and 3-penten-2-one (**2a**).

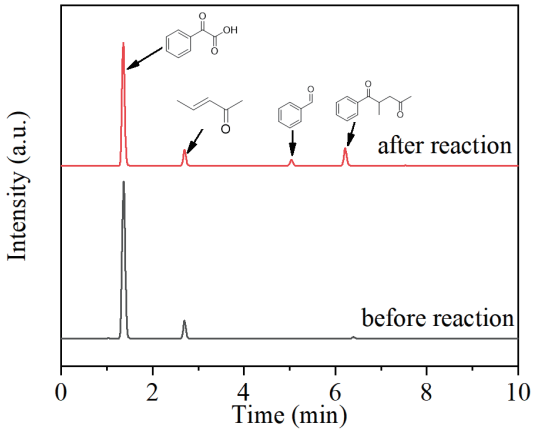

FIG. 7 Representative liquid chromatogram of the sample solution before and after the photocatalytic reaction.

methyl-1-phenylpentane-1,4-dione, **3a**) and hydrogenated product (benzaldehyde, **4a**) were observed, as shown in the representative liquid chromatogram (FIG. 7). The peaks at 1.35 and 2.7 min correspond to substrates, namely PhCOCOOH and 3-penten-2-one, respectively. Additionally, the peaks with retention time of 5.04 and 6.22 min were attributed to benzaldehyde and the acylation products, respectively.

The calibration curve of PhCOCOOH was made based on the corresponding peak area of liquid chromatogram and used for quantification of reacted amount of PhCOCOOH during photocatalytic reaction. The reeaction condition: PhCOCOOH (0.028 mmol), 3-penten-2-one (1.5 e.q.), photocatalyst (1 mol%), Na_2HPO_4/NaH_2PO_4 (37.5 mmol/L), CH_3CN (0.35 mL)/H_2O (0.35 mL), 300 mW 450 nm at room temperature for 40 min under argon atmosphere.

$$\Phi = \frac{\text{mole of reacted substrate}}{\text{mole of absorbed photons}} \times 100\% = \frac{n_r hcN_A}{I_{abs} t\lambda} \times 100\% \quad (10)$$

where Φ is the quantum yield of the photocatalytic reaction; n_r is the reacted benzoylformic acid in mole; I_{abs} is the absorbed light power by the solution in watt; t is the duration of light illumination in second; λ is the wavelength of the light source in meter; h is the Planck constant, 6.62×10^{-34} J·s; c is the speed of light, 3.0×10^8 m/s; N_A is the Avogadro constant, 6.022×10^{23} mol^{-1}.

TABLE II Steady-state efficiency of photocatalytic conversion of PhCOCOOH.

Entry	Photocatalyst	Conversion[a] /%	Quantum yield[b]/%
1	IrIII	45	0.63
2	Eosin Y	3.4	0.054
3	Rose Bengal	7.4	0.086
4	4CzPN	3.0	0.032

[a] Conversion was calculated based on the reacted amount of benzoylformic acid measured by UPLC.
[b] Quantum yield was calculated by Eq.(10).

For all the photocatalysts tested, IrIII exhibits the highest conversion rate of benzoylformic acid as 45% (Table II, entry 1), significantly outperforming the other three photocatalysts (Table II). To take into account the difference of light power absorbed by different photocatalysts and thus better correlate the steady-state efficiency with the transient kinetics, we further quantify the quantum yield (QY) of photocatalytic reaction based on the conversion of PhCOCOOH according to Eq.(10). The light power impinging on and transmitting through the cuvette reactor were measured via a power meter with thermal sensor (Thorlab PM160T) and thus the light power absorbed by the PCs (I_{abs}) was obtained by subtracting the impinging light power from the transmitting one. The results in Table II revealed that the IrIII still exhibits the highest quantum yield among the four photocatalysts, achieving 0.63%. The QYs of the photocatalysts are ranked as IrIII>RBH>EYH>4CzPN, in good accordance with the quenching efficiency of electronically excited photocatalysts by PhCOCOOH observed in transient spectroscopy experiments (Table I). This supports the conclusion that IrIII and RBH, with triplet states as their catalytically active excited states, may exhibit higher photocatalytic efficiency, particularly under anaerobic

DOI: 10.1063/1674-0068/cjcp2407098

conditions. The gap between the absolute values of quantum yield measured from steady-state photocatalytic reaction and transient quenching experiments is likely due to the existence of back-electron-transfer event after the single electron transfer induced by photoexcitation.

IV. SUMMARY

In this study, we employed time-resolved absorption and emission spectroscopy to thoroughly characterize the key quenching steps of photocatalysts, including the transition metal complex $[Ir(dFCF_3ppy)_2(dtbbpy)]^+$ (IrIII) and the organic small molecules Eosin Y (EY), Rose Bengal (RB), and 4CzPN, in promoting the radical acylation of α-keto acids. Our results demonstrate that the catalytically active excited state of RB is its protonated triplet state (^{3}RBH*: $\Phi_{ISC}=0.77$; $k_{air}=9.7\times10^6$ s^{-1}, $k_{N_2}=2.9\times10^5$ s^{-1}), while both EY and 4CzPN show catalytic activity in its singlet state (^{1}EYH*: $k=3.4\times10^8$ s^{-1}; ^{1}4CzPN*: $k=2.0\times10^8$ s^{-1}). We further measured the second-order reaction rate constants for the quenching of these catalytically active excited states by the α-keto acid substrates (^{1}EYH*: 2.3×10^9 (mol/L)$^{-1}\cdot$s^{-1}; ^{3}RBH*: 3.2×10^8 (mol/L)$^{-1}\cdot$s^{-1}; ^{1}4CzPN*: 2.8×10^8 (mol/L)$^{-1}\cdot$s^{-1}). Using these kinetic data, together with the results recently reported by our group for IrIII (^{3}IrIII*: $\Phi_{ISC}=1$; $k_{air}=5.0\times10^6$ s^{-1}, $k_{N_2}=4.3\times10^5$ s^{-1}; 2.8×10^7 (mol/L)$^{-1}\cdot$s^{-1}), we established a relationship between substrate concentration and excited-state quenching efficiency for these four photocatalysts both under aerobic and anaerobic conditions. We found that key factors influencing the quenching efficiency include the intrinsic lifetime of the excited state, the quantum yield of the catalytically active excited state, its susceptibility to oxygen, and the second-order reaction rate constant with the substrate.

Meanwhile, through steady-state chromatography measurements, we measured the quantum efficiencies of the photocatalytic decarboxylation of PhCOCOOH for these four photocatalysts (IrIII > RBH > EYH > 4CzPN), and established correlations between the efficiencies and initial quenching process, which suggest IrIII and RBH, with triplet states as their catalytically active excited states, may exhibit higher photocatalytic efficiency, particularly under anaerobic conditions. Considering that the quantum efficiency of the entire catalytic cycle for the radical acylation of α-keto acids is largely affected by the quenching efficiency of the initial step, our analysis of substrate concentration-dependent quenching efficiency provides a foundation for understanding the catalytic quantum efficiency of different photosensitizers. We note that, in addition to the quenching efficiency of the initial step, factors such as cage escape quantum yields, solvent polarity, and subsequent back electron transfer also affect the overall efficiency of the photocatalytic cycle. Future work is strongly encouraged to investigate the effects of these factors on quantum efficiency.

V. ACKNOWLEDGMENTS

This work was supported by the National Key R&D Program of China (No.2022YFA1505400), the National Natural Science Foundation of China (Nos. 21933005, 21727803, 22003005 and 22273007), and the Fundamental Research Funds for the Central Universities (No.2233300007).

[1] C. Chatgilialoglu, D. Crich, M. Komatsu, and I. Ryu, Chem. Rev. **99**, 1991 (1999).
[2] F. Penteado, E. F. Lopes, D. Alves, G. Perin, R. G. Jacob, and E. J. Lenardão, Chem. Rev. **119**, 7113 (2019).
[3] N. A. Romero and D. A. Nicewicz, Chem. Rev. **116**, 10075 (2016).
[4] J. Liu, Q. Liu, H. Yi, C. Qin, R. P. Bai, X. T. Qi, Y. Lan, and A. W. Lei, Angew. Chem. Int. Ed. **53**, 502 (2014).
[5] W. M. Cheng, R. Shang, H. Z. Yu, and Y. Fu, Chem. Eur. J. **21**, 13191 (2015).
[6] L. L. Chu, J. M. Lipshultz, and D. W. C. MacMillan, Angew. Chem. Int. Ed. **54**, 7929 (2015).
[7] G. Z. Wang, R. Shang, W. M. Cheng, and Y. Fu, Org. Lett. **17**, 4830 (2015).
[8] C. Zhou, P. H. Li, X. J. Zhu, and L. Wang, Org. Lett. **17**, 6198 (2015).
[9] L. J. Gu, C. Jin, J. Y. Liu, H. T. Zhang, M. L. Yuan, and G. P. Li, Green Chem. **18**, 1201 (2016).
[10] N. Xu, P. H. Li, Z. G. Xie, and L. Wang, Chem. Eur. J. **22**, 2236 (2016).
[11] Q. F. Bai, C. G. Jin, J. Y. He, and G. F. Feng, Org. Lett. **20**, 2172 (2018).
[12] A. Banerjee, Z. Lei, and M. Y. Ngai, Synthesis **51**, 303 (2019).
[13] Y. F. Lv, P. L. Bao, H. L. Yue, J. S. Li, and W. Wei, Green Chem. **21**, 6051 (2019).
[14] X. F. Zhang, P. Y. Zhu, R. H. Zhang, X. Li, and T. L.

DOI: 10.1063/1674-0068/cjcp2407098

Yao, J. Org. Chem. **85**, 9503 (2020).
[15] D. L. Zhu, Q. Wu, D. J. Young, H. Wang, Z. G. Ren, and H. X. Li, Org. Lett. **22**, 6832 (2020).
[16] B. Yang, S. J. Li, Y. D. Wang, Y. Lan, and S. F. Zhu, Nat. Commun. **12**, 5257 (2021).
[17] J. Li, X. C. Lu, Y. Xu, J. X. Wen, G. Q. Hou, and L. Liu, Org. Lett. **22**, 9621 (2020).
[18] J. L. Tucker, Org. Process Res. Dev. **10**, 315 (2006).
[19] S. Ruccolo, Y. Z. Qin, C. Schnedermann, and D. G. Nocera, J. Am. Chem. Soc. **140**, 14926 (2018).
[20] L. Flamigni, A. Barbieri, C. Sabatini, B. Ventura, and F. Barigelletti, *Photochemistry and Photophysics of Coordination Compounds II*, V. Balzani and S. Campagna Eds., Berlin, Heidelberg: Springer, 143 (2007). DOI: 10.1007/128_2007_131.
[21] G. J. Hedley, A. Ruseckas, and I. D. W. Samuel, J. Phys. Chem. A **114**, 8961 (2010).
[22] S. Tschierlei, A. Neubauer, N. Rockstroh, M. Karnahl, P. Schwarzbach, H. Junge, M. Beller, and S. Lochbrunner, Phys. Chem. Chem. Phys. **18**, 10682 (2016).
[23] Z. C. Lin, Q. Zhou, Y. Liu, C. L. Chen, J. L. Jie, and H. M. Su, Chem. Sci. **15**, 11919 (2024).
[24] D. A. Nicewicz and T. M. Nguyen, ACS Catal. **4**, 355 (2014).
[25] S. G. E. Amos, M. Garreau, L. Buzzetti, and J. Waser, Beilstein J. Org. Chem. **16**, 1163 (2020).
[26] F. Herbrik, P. Camarero González, M. Krstic, A. Puglisi, M. Benaglia, M. A. Sanz, and S. Rossi, Appl. Sci. **10**, 5596 (2020).
[27] V. R. Batistela, D. S. Pellosi, F. D. de Souza, W. F. da Costa, S. M. de Oliveira Santin, V. R. de Souza, W. Caetano, H. P. M. de Oliveira, I. S. Scarminio, and N. Hioka, Spectrochim. Acta Part A: Mol. Biomol. Spectrosc. **79**, 889 (2011).
[28] S. Sharma and A. Sharma, Org. Biomol. Chem. **17**, 4384 (2019).
[29] T. Shen, Z. G. Zhao, Q. Yu, and H. J. Xu, J. Photochem. Photobiol. A: Chem. **47**, 203 (1989).
[30] A. Srivastava, P. K. Singh, A. Ali, P. P. Singh, and V. Srivastava, RSC Adv. **10**, 39495 (2020).
[31] H. Uoyama, K. Goushi, K. Shizu, H. Nomura, and C. Adachi, Nature **492**, 234 (2012).
[32] J. Luo and J. Zhang, ACS Catal. **6**, 873 (2016).

DOI: 10.1063/1674-0068/cjcp2407098